

Exploring the physics of the accretion and jet in nearby narrow-line Seyfert 1 galaxies

Su Yao¹★, Erlin Qiao^{2,3}, Xue-Bing Wu^{1,4}, B. You^{5,6}

¹Kavli Institute for Astronomy and Astrophysics, Peking University, Beijing 100871, China

²National Astronomical Observatories, Chinese Academy of Sciences, Beijing 100012, China

³School of Astronomy and Space Sciences, University of Chinese Academy of Sciences, 19A Yuquan Road, Beijing 100049, China

⁴Department of Astronomy, School of Physics, Peking University, Beijing 100871, China

⁵School of Physics and Technology, Wuhan University, Wuhan 430072, China

⁶Copernicus Astronomical Center, Polish Academy of Science, Bartyczna 18, 00-716 Warsaw, Poland

Accepted XXX. Received YYY; in original form ZZZ

ABSTRACT

In this paper, we explore the physics of the accretion and jet in narrow-line Seyfert 1 galaxies (NLS1). Specifically, we compile a sample composed of 16 nearby NLS1 with $L_{\text{bol}}/L_{\text{Edd}} \gtrsim 0.1$. We investigate the mutual correlation between their radio luminosity L_{R} , X-ray luminosity L_{X} , optical luminosity L_{5100} and black hole mass M_{BH} . By adopting partial correlation analysis: (1) we find a positive correlation between L_{X} and M_{BH} , and (2) we find a weak positive correlation between L_{R} and L_{5100} . However, we don't find significant correlations between L_{R} and L_{X} or between L_{X} and L_{5100} after considering the effect of the black hole mass, which leads to a finding of the independence of $L_{\text{X}}/L_{\text{Edd}}$ on L_{5100}/L_{Edd} . Interestingly, the findings that L_{X} is correlated with M_{BH} and $L_{\text{X}}/L_{\text{Edd}}$ is not correlated with L_{5100}/L_{Edd} support that the X-ray emission is saturated with increasing \dot{M} for $L_{\text{bol}}/L_{\text{Edd}} \gtrsim 0.1$ in NLS1s, which may be understood in the framework of slim disc scenario. Finally, we suggest that a larger NLS1 sample with high quality radio and X-ray data is needed to further confirm this result in the future.

Key words: galaxies: active – galaxies: nuclei – galaxies: Seyfert – accretion, accretion discs – galaxies: jets

1 INTRODUCTION

Narrow-line Seyfert 1 galaxy (NLS1) is a subclass of broad-line active galactic nuclei (AGNs), identified optically by full width at half maximum (FWHM) of their broad H β emission line $< 2000 \text{ km s}^{-1}$ and weak [O III] lines with $[\text{O III}]\lambda 5007/\text{H}\beta < 3$ (Osterbrock & Pogge 1985; Goodrich 1989). Compared to normal Seyfert 1 galaxies, NLS1s show smaller FWHM(H β), weaker [O III], stronger Fe II emission, stronger blueshift of the [O III] and C IV, steeper soft X-ray spectrum (e.g., Boroson & Green 1992; Véron-Cetty et al. 2001; Sulentic et al. 2000, 2007; Leighly & Moore 2004; Wang et al. 1996; Boller et al. 1996). NLS1s are located at an extreme end of a correlation matrix of AGN observables, which is believed to be driven mainly by the Eddington ratio $L_{\text{bol}}/L_{\text{Edd}}$ (e.g., Boroson & Green 1992; Boroson 2002), where L_{bol} is the bolometric luminosity and $L_{\text{Edd}} = 1.3 \times 10^{38} M_{\text{BH}}/M_{\odot} \text{ erg s}^{-1}$. Bulk of the black hole masses of the NLS1s has been measured to be $\sim 10^{6-7} M_{\odot}$ by various methods [e.g., the reverberation mapping method (e.g., Wang et al. 2014) and the luminosity-radius relation (e.g., Zhou et al. 2006)]. They

generally have high Eddington ratios close to or even above unity, so they are often suggested to be powered by slim discs (e.g., Wang & Zhou 1999; Mineshige et al. 2000).

NLS1s are often being radio-quiet¹ compared with other broad-line AGNs (e.g., Ulvestad et al. 1995; Stepanian et al. 2003; Whalen et al. 2006). Only $\sim 7\%$ of the optical selected NLS1s are radio-loud (e.g., Komossa et al. 2006; Zhou et al. 2006), while this fraction is $10\% - 15\%$ for normal broad-line AGNs (Ivezić et al. 2002). By performing a comprehensive study of 23 genuine radio-loud NLS1s selected from a large NLS1 sample, Yuan et al. (2008) have found evidence of relativistic blazar-like jet in the radio loudest NLS1s. Then the powerful jet in the radio-loud NLS1s was confirmed by the γ -ray detections (e.g., Abdo et al. 2009a,b; D'Ammando et al. 2012; Yao et al. 2015). On the other hand, several works have found the evidence for the presence of jets in some radio-quiet NLS1s revealed by VLBI images, e.g., extended jet-like features and high brightness temperatures of the compact radio core

¹ A measurement of the radio loudness is usually characterized by a parameter $R = f_{5\text{GHz}}/f_{4400}$, where $f_{5\text{GHz}}$ and f_{4400} are the flux densities at 5 GHz and 4400 Å. The optically selected AGNs can be conventionally classified as radio-quiet if $R \lesssim 10$ (Kellermann et al. 1989).

★ E-mail: yaosu@pku.edu.cn

component on pc scales (e.g., Lal et al. 2004; Giroletti & Panessa 2009; Doi et al. 2013, 2015).

Generally, the X-ray emission in radio-quiet AGNs is believed to be produced in the hot corona by the inverse Compton scattering of the soft photons from the accretion disc (e.g., Haardt & Maraschi 1991, 1993; Liu et al. 2002), while the origin of the radio emission in the radio-quiet AGNs is still not fully understood, which is suggested to be from jets by some works although not fully proved (e.g., Czerny & You 2016). It is shown that the study of the relation between the radio luminosity and X-ray luminosity is a very useful tool to investigate the coupling of the accretion and the jet (Merloni et al. 2003). The radio/X-ray correlation has been investigated for different types of AGN, as well as black hole X-ray binaries (BHBs) in the low/hard spectral state (e.g., Merloni et al. 2003; Wang et al. 2006; Li et al. 2008; de Gasperin et al. 2011). It is found that $L_{5\text{GHz}} \propto L_{2-10\text{keV}}^{-0.5-0.7}$ in the low-luminosity AGNs (LLAGNs) and in the under-luminous low/hard spectral state of BHBs (e.g., Körding et al. 2006), while this correlation becomes significantly steeper, i.e., $L_{5\text{GHz}} \propto L_{2-10\text{keV}}^{-1.4}$, in the luminous AGNs and the luminous low/hard spectral state of BHBs (e.g., Corbel et al. 2004; Rushton et al. 2010; Dong et al. 2014).

Some NLS1s have been included in previous studies of radio/X-ray correlation. However, due to that the number of the NLS1s in the sample is very small, their statistical properties are overwhelmed by other types of AGNs. (e.g., Merloni et al. 2003; Dong et al. 2014; Panessa et al. 2015). Furthermore, the measurements of their radio luminosities could be severely contaminated by the host galaxies, e.g., if the resolution of the radio observation is not high enough, the star formation activities in their circum-nuclear regions can have very strong contributions to the radio luminosity (e.g., Deo et al. 2006; Ohta et al. 2007; Sani et al. 2010). Caccianiga et al. (2015) found that the star formation activities can contribute a significant fraction of VLA/FIRST radio emission even in some radio-loud NLS1s. In order to reduce the contaminations from the host galaxy as much as possible, in this work we make use of radio fluxes within the central regions ($\lesssim 1$ kpc) of nearby radio-quiet NLS1s measured from high resolution radio images, to study their nuclear radio/X-ray relation which was rarely studied before. This could help us understand the physics of the accretion and jet in high Eddington ratio regime. We also explore the mutual relation between the radio luminosity, X-ray luminosity, optical luminosity and black hole mass. There are several works on the radio images of radio loud NLS1s on kpc scales or even pc scales recently (e.g., Doi et al. 2011, 2012; Gu et al. 2015). But we do not choose the radio loud ones as to avoid the relativistically beaming effects. Throughout this work a cosmology is assumed with $H_0 = 70$ km s $^{-1}$ Mpc $^{-1}$, $\Omega_\Lambda = 0.73$ and $\Omega_M = 0.27$. The luminosities taken from literatures would be transformed to the cosmology used here when necessary.

2 THE SAMPLE

2.1 Sample selection

We select objects from the 13th edition of the catalogue of quasars and active galactic nuclei compiled by Véron-Cetty & Véron (2010), including both quasars (defined as brighter than absolute magnitude $M_B = -22.25$) and Seyfert galaxies (fainter than $M_B = -22.25$), with criteria as follows.

(i) The object is classified as NLS1 with redshift $z < 0.1$ according to its optical spectroscopy.

(ii) The object is radio-quiet.

(iii) The object is detected by the high-resolution radio observations within the central nuclear region less than about 1 kpc.

(iv) The object has an Eddington ratio of $L_{\text{bol}}/L_{\text{Edd}} \gtrsim 0.1$.

The criterion of being classified as NLS1 in Véron-Cetty & Véron (2010) is that the FWHM of the H β emission line broad component is narrower than 2000 km s $^{-1}$. 265 NLS1s are picked out at this step. Then, we search for the corresponding radio observations by VLA of the selected NLS1s with an angular resolution corresponding to a physical size of $\lesssim 1$ kpc at the object's rest frame from the literatures, i.e., Ulvestad & Wilson (1984b), Miller et al. (1993), Kukula et al. (1995), Ulvestad et al. (1995), Kukula et al. (1998), Kinney et al. (2000), Schmitt et al. (2001), Ho & Ulvestad (2001), Lal et al. (2004), Orienti & Prieto (2010) and Parra et al. (2010). After this step, we have 17 sources left.

We estimate the Eddington ratios for these 17 sources (see section 2.4 for details). All of them have $L_{\text{bol}}/L_{\text{Edd}} > 0.1$ except for NGC 4051. The nuclear continuum flux at 5100 Å of NGC 4051 is about 5×10^{-15} erg s $^{-1}$ cm $^{-2}$ after subtracting the host galaxy starlight and its black hole mass estimated from the reverberation mapping method is $1.73 \times 10^6 M_\odot$ (Denney et al. 2009). The Eddington ratio is $\sim 1\%$ for NGC 4051. Thus we exclude it from our sample. The final sample consists of 16 NLS1s with $z < 0.1$ and $L_{\text{bol}}/L_{\text{Edd}} > 0.1$ (Table 1). None of them are reported to be radio-loud in previous works (e.g., Komossa et al. 2006; Yuan et al. 2008; Foschini et al. 2015). In the work of Berton et al. (2015), the radio loudness of Mrk 1239 and Mrk 766 have been reported as 16 and 23, respectively. They could be classified as so-called radio-intermediate AGNs instead of genuine radio-loud ones (Falcke et al. 1996), which are also included in our sample. Here we should note that this sample is not complete, since we only select sources that are detected in high resolution radio observations. But this is the largest sample we can find from the literatures at this stage.

2.2 Radio luminosity

We collect the radio flux for each source from the references listed in Column (5) of Table 1. They usually have steep radio spectra ($\alpha_r < -0.5$, where $S_\nu \propto \nu^{\alpha_r}$), not remarkably different from the normal Seyfert 1 galaxies (Miller et al. 1993; Ulvestad et al. 1995). As shown by the radio images given in these references, most of the sources have compact and unresolved morphology within a few hundred pc in central region. A few exceptions exist, e.g., Mrk 110 and Mrk 1239 show extended features on kpc-scales (Miller et al. 1993; Kellermann et al. 1994; Doi et al. 2015), and Ark 564 has a triple radio component along the north-south direction (Thean et al. 2001).

We calculate the core radio luminosities from their peak flux densities of the core component. The observations were performed at different frequencies. We always use the flux density observed at ~ 5 GHz if available. When the observation was taken at other frequencies, the flux is extrapolated from the observing center frequency to 5 GHz using the radio spectral index if available or using an typical spectral index of $\alpha_r = -0.7$ (e.g., Doi et al. 2013). The luminosities are listed in Table 1. A typical value of $\sigma_R = 0.2$ dex (Ho & Peng 2001) is adopted as the uncertainty of the radio luminosity.

Six of these objects, namely, Mrk 110, Mrk 705, Mrk 783, Mrk 766 (Doi et al. 2013), Mrk 1239 (Doi et al. 2013, 2015) and

Table 1. Radio, X-ray and optical luminosities of the radio-quiet NLS1 sample with the measured black hole masses.

Name	z	$\log L_R$ VLA (ergs s ⁻¹)	size (pc)	Ref.	$\log L_R$ VLBI (ergs s ⁻¹)	size (pc)	Ref.	$\log L_X$ 2 – 10 keV (ergs s ⁻¹)	Ref.	$\log L_{HX}$ 14 – 195 keV (ergs s ⁻¹)	$\log M_{BH}$ (M_\odot)	$\log L_{5100}$ (ergs s ⁻¹)	Ref.	λ
(1)	(2)	(3)	(4)	(5)	(6)	(7)	(8)	(9)	(10)	(11)	(12)	(13)	(14)	(15)
Mrk 335	0.0258	38.31	152	1	-	-	-	43.17	10,11,12,13	43.45	6.92	43.60	43,M	0.38
I Zw 1	0.0611	38.71	385	1	-	-	-	43.72	14,15,16,17	-	7.26	44.51	44,S	1.40
Mrk 359	0.0168	37.36	170	2	-	-	-	42.60	18,19,20	42.93	5.48	41.99 ^b	45,S	0.25
Mrk 110	0.0353	38.42	320	3	37.86	7.5	9	43.83	10,21,22	44.22	7.05	43.61	43,M	0.28
Mrk 705	0.0292	38.45	< 55	4	37.91	6.5	9	43.48	23,24	43.49	6.79	43.04 ^b	45,46,S	0.14
Mrk 1239	0.0199	38.93	140	5	37.70	4.5	9	43.02	25	43.05 ^a	6.11	43.27	47,S	1.12
Mrk 766	0.0129	38.41	95	6	37.04	2.9	9	42.84	21,24,26, 17,27,28	42.91	6.11	42.53	48,M	0.20
PG 1244+026	0.0481	38.13	434	3	-	-	-	43.17	14,17,29	-	6.28	43.43	44,S	1.11
Mrk 783	0.0672	39.27	< 380	7	38.54	13.6	9	43.84	30	44.28	7.16	43.91 ^a	49,S	0.44
PG 1404+226	0.0983	38.95	837	3	-	-	-	42.88	14,17	-	6.89	44.38	50,S	2.40
Mrk 478	0.0790	38.76	688	3	-	-	-	43.84	14,17,31,32	-	7.37	44.48	44,S	1.02
PG 1448+273	0.0645	38.76	571	3	-	-	-	43.33	32	-	7.01	44.01	44,S	0.77
IRAS 1509–211	0.0445	39.44	< 830	5	-	-	-	43.57	33,34,35	44.16	7.00	43.98	51,S	0.74
Mrk 493	0.0310	37.92	< 260	5	-	-	-	42.95	19	-	6.18	43.03	43,M	0.55
Mrk 507	0.0559	38.70	< 1320	5	-	-	-	42.81	19,36,37	43.56	6.91	43.77	51,S	0.56
Ark 564	0.0247	38.93	320	8	38.40	1.2	8	43.36	21,31,38,39, 40,41,42	43.52 ^a	6.42	43.68	52,S	1.44

^a This luminosity is converted from 10 – 50 keV measured by *Suzaku*/HXD (Fukazawa et al. 2011) assuming a photon index of $\Gamma = 2$.

^b This monochromatic luminosity is estimated from $L_{H\beta} - L_{5100}$ relation of Greene & Ho (2005) and $L_{H\beta}$ is obtained from the corresponding references in Column (14).

Note. Column (1): source name. Column (2): source redshift. Column (3): the VLA monochromatic radio luminosity at 5 GHz. Column (4): the linear size of the emitting region from which Column (3) is measured. Column (5): the references for Column (3) and (4). Column (6): the VLBI monochromatic radio luminosity at 5 GHz, Column (7): the linear size of the emitting region from which Column (6) is measured. Column (8): the references for Column (6) and (7). Column (9): the average X-ray luminosity in the 2 – 10 keV band. Column (10): the references for Column (9). Column (11): the hard X-ray luminosity in the 14 – 195 keV band taken from the 70 month *Swift*/BAT survey (Baumgartner et al. 2013), except for Mrk 1239 and Ark 564, for which the hard X-ray luminosity in the 10 – 50 keV was taken from Fukazawa et al. (2011), and then converted to the 14 – 195 keV band. Column (12): the black hole masses. Column (13): monochromatic nuclear luminosity at 5100 Å. Column (14): references for the M_{BH} and L_{5100} . The black hole masses are derived from the reverberation mapping method (M) or single-epoch spectroscopy (S). Column (15): Eddington ratio.

References: (1) Kukula et al. (1995); (2) Kinney et al. (2000); (3) Miller et al. (1993); (4) Schmitt et al. (2001); (5) Ulvestad et al. (1995); (6) Parra et al. (2010); (7) Ulvestad & Wilson (1984a); (8) Lal et al. (2004); (9) Doi et al. (2013); (10) George et al. (2000); (11) Grupe et al. (2007); (12) Grupe et al. (2010); (13) Keek & Ballantyne (2016); (14) Piconcelli et al. (2005); (15) Reeves & Turner (2000); (16) Costantini et al. (2007); (17) Ueda et al. (2001); (18) Lutz et al. (2004); (19) Bianchi et al. (2009); (20) Boissay et al. (2016); (21) Nandra et al. (2007); (22) Winter et al. (2012); (23) Gallo et al. (2005); (24) Shu et al. (2010); (25) Grupe et al. (2004); (26) Matt et al. (2000); (27) Landi et al. (2005); (28) Giachè et al. (2014); (29) Jin et al. (2013); (30) Panessa et al. (2011); (31) Shinozaki et al. (2006); (32) Inoue et al. (2007); (33) Brightman & Nandra (2011); (34) Liu et al. (2014); (35) Liu et al. (2015); (36) Iwasawa et al. (1998); (37) de La Calle Pérez et al. (2010); (38) Turner et al. (2001); (39) Vignali et al. (2004); (40) Matsumoto et al. (2004); (41) Papadakis et al. (2007); (42) Ramírez (2013); (43) Wang et al. (2014); (44) Wang et al. (2013); (45) Ho et al. (2008); (46) Marziani et al. (2003); (47) Ryan et al. (2007); (48) Grier et al. (2013); (49) Wang & Lu (2001); (50) Vestergaard & Peterson (2006); (51) Ohta et al. (2007); (52) Botte et al. (2004);

Ark 564 (Lal et al. 2004), have also been detected by VLBI observations and exhibit radio core with angular size of a few milliarc-second, corresponding to a linear size of only a few pc. The sources show clear elongated features extending to one side or both sides of the core with a brightness peak. In addition, their core components have high brightness temperatures of $T_B \gtrsim 10^7$ K (Doi et al. 2013; Lal et al. 2004). The VLBI luminosities of the sources are also listed in the table.

2.3 X-ray luminosity

For the X-ray luminosities, we have searched NASA/IPAC Extragalactic Database (NED) and literatures in which the 2–10 keV fluxes or luminosities of the selected NLS1s are reported (Column 10 in Table 1). The selected objects are all nearby with $z < 0.1$ and relatively bright in the X-rays. The central AGN is generally 2–3 orders of magnitude more luminous than the typical level of X-ray sources of the host galaxy, e.g., X-ray binaries and supernova remnants (Fabbiano 1989).

The fluxes are corrected for the Galactic absorption before converted to luminosities. For most of the sources in the sample, the spectral analysis results given in the literatures show weak intrinsic absorption with $N_H < 10^{22}$ cm⁻², which consequently will not significantly affect the hard X-ray flux in our study. Piconcelli et al. (2005) reported an intrinsic gas column density of $N_H = 1.4 \times 10^{22}$ cm⁻² for PG 1404+226 from the spectral fit, which will lead to an underestimation of the 2–10 keV luminosity by ~ 16 percent for a spectrum with $\Gamma = 2$. Another peculiar object worth mentioning is Mrk 507. This source has a very strong Fe II with $R_{4570} = 1.94$ (Véron-Cetty et al. 2001), on the other hand, it exhibits a flat *ROSAT* 0.1 – 2.4 keV spectrum with $\Gamma = 1.6$ which was suggested to be caused by intrinsic absorption with a column density of $N_H = (2 - 3) \times 10^{21}$ cm⁻² (Iwasawa et al. 1998). Its *ROSAT* spectrum is still flat ($\Gamma \sim 2.4$) even after correction of intrinsic absorption (Iwasawa et al. 1998). With a extremely strong Fe II and the flattest soft X-ray spectrum, Mrk 507 is unusual in the light of positive correlation between the Fe II strength and the steepness of *ROSAT* spectrum (Wang et al. 1996). However, the suggested in-

trinsic absorption should have little affection (a few percent) to the X-rays above 2 keV. Nevertheless, we adopt the flux reported in literatures after correction of only Galactic absorption for all the sources.

We note here that the X-ray variability is very common in AGNs and its variability amplitude usually ranges from a few times to more than an order of magnitude on timescales of months up to years (e.g., Mushotzky et al. 1993). The measurement of the X-ray and other observables at different epochs may lead to large uncertainties when studying their relation. So we take the unweighted mean X-ray flux when multiple observations are available for each source. Although there are significant X-ray variabilities between different X-ray observations for individual sources, they varied within an order of magnitude. The photon indices of the 2–10 keV spectra of the sample are in the range of $\Gamma \sim 1.6 - 2.9$ and do not varied much either ($\Delta\Gamma \lesssim 0.5$) for individual sources². Four of these objects, Mrk 110, Mrk 335, Mrk 705 and Ark 564 have been monitored by *RXTE*/ASM and/or by *MAXI*. We check the ASM and *MAXI* 1-day-binned light curves, and find that the sources have not been detected for most of the time. Only in few cases the light curve demonstrated flares where the fluxes increase possibly by more than an order of magnitude. The value of 2–10 keV fluxes of each source we adopted here do not vary as large as during the flares, so they were most probably in their typical flux state during the observations. We adopt the range between highest and lowest values as the uncertainty for each source if there are multiple X-ray observations. If there is only one X-ray observation, a typical uncertainty of $\sigma_X = 0.23$ dex is adopted (Strateva et al. 2005).

Eight sources in the sample are reported in the Swift-BAT 70-Month catalog (Baumgartner et al. 2013). For another two sources such as Mrk 1239 and Ark 564, X-ray luminosities are converted from 10–50 keV measured by *Suzaku*/HXD (Fukazawa et al. 2011) to 14–195 keV assuming a photon index of $\Gamma = 2$ and $\sigma_X = 0.23$ dex for these two sources (see Column 11 of Table 1).

2.4 Black hole mass and Eddington ratio

Some of the NLS1s in the sample are included in large reverberation-mapping campaigns (e.g., Grier et al. 2013; Wang et al. 2014), in which the black hole masses are estimated by measuring the structure of the broad-line region using mapping technique. For the rest of the sources, their black hole masses are estimated with the line width-luminosity mass scaling relation using single-epoch optical spectroscopy (see column 14 of Table 1). The black hole masses are in the range of $10^{5.5-7.4} M_\odot$, as the typical value of NLS1 population (Zhou et al. 2006).

The Eddington ratio of the NLS1s studied here were estimated in numerous works (e.g., Wang et al. 2014; Ohta et al. 2007; Marziani et al. 2003; Ho et al. 2008; Grier et al. 2013; Wang & Lu 2001; Ryan et al. 2007; Botte et al. 2004). All of the results support that these sources are accreting close to or above Eddington limit. We simply estimate their Eddington ratios $\lambda = L_{\text{bol}}/L_{\text{Edd}}$ (Column 15 in Table 1) assuming $L_{\text{bol}} = 9.8L_{5100}$ (McLure & Dunlop 2004), where L_{5100} is the monochromatic luminosities at 5100 Å. For most of the sources in the sample, the L_{5100} are calculated from

Table 2. Results of correlation analysis.

Variables			Correlation	
X	Y	Z	τ	P_{null}
(1)	(2)	(3)	(4)	(5)
$\log L_{X,2-10\text{keV}}$	$\log L_{R,VLA}$	$\log M_{\text{BH}}$	0.14	0.47
$\log L_{X,2-10\text{keV}}$	$\log L_{R,VLBI}$	$\log M_{\text{BH}}$	0.31	0.45
$\log L_{X,14-195\text{keV}}$	$\log L_{R,VLA}$	$\log M_{\text{BH}}$	0.37	0.17
$\log L_{X,14-195\text{keV}}$	$\log L_{R,VLBI}$	$\log M_{\text{BH}}$	0.59	0.15
$\log L_{R,VLA}$	$\log L_{5100}$	$\log M_{\text{BH}}$	0.39	0.04
$\log L_{R,VLBI}$	$\log L_{5100}$	$\log M_{\text{BH}}$	0.62	0.13
$\log L_{X,2-10\text{keV}}$	$\log L_{5100}$	$\log M_{\text{BH}}$	-0.02	0.94
$\log L_{X,14-195\text{keV}}$	$\log L_{5100}$	$\log M_{\text{BH}}$	0.42	0.12
$\log L_{X,2-10\text{keV}}$	$\log L_{R,VLA}$	$\log L_{5100}$	0.14	0.47
$\log L_{X,2-10\text{keV}}$	$\log L_{R,VLBI}$	$\log L_{5100}$	0.29	0.47
$\log L_{X,14-195\text{keV}}$	$\log L_{R,VLA}$	$\log L_{5100}$	-0.02	0.95
$\log L_{X,14-195\text{keV}}$	$\log L_{R,VLBI}$	$\log L_{5100}$	0.42	0.30
$\log L_{R,VLA}$	$\log M_{\text{BH}}$	$\log L_{5100}$	0.01	0.97
$\log L_{R,VLBI}$	$\log M_{\text{BH}}$	$\log L_{5100}$	0.26	0.52
$\log L_{R,VLA}$	$\log M_{\text{BH}}$	$\log L_{X,2-10\text{keV}}$	0.20	0.31
$\log L_{R,VLBI}$	$\log M_{\text{BH}}$	$\log L_{X,2-10\text{keV}}$	-0.13	0.74
$\log L_{R,VLA}$	$\log M_{\text{BH}}$	$\log L_{X,14-195\text{keV}}$	-0.07	0.78
$\log L_{R,VLBI}$	$\log M_{\text{BH}}$	$\log L_{X,14-195\text{keV}}$	-0.14	0.72
$\log L_{X,2-10\text{keV}}$	$\log M_{\text{BH}}$	$\log L_{5100}$	0.52	7.28×10^{-3}
$\log L_{X,2-10\text{keV}}$	$\log M_{\text{BH}}$	$\log L_{R,VLA}$	0.58	2.47×10^{-3}
$\log L_{X,2-10\text{keV}}$	$\log M_{\text{BH}}$	$\log L_{R,VLBI}$	0.95	0.02
$\log L_{X,14-195\text{keV}}$	$\log M_{\text{BH}}$	$\log L_{5100}$	0.59	0.03
$\log L_{X,14-195\text{keV}}$	$\log M_{\text{BH}}$	$\log L_{R,VLA}$	0.74	5.79×10^{-3}
$\log L_{X,14-195\text{keV}}$	$\log M_{\text{BH}}$	$\log L_{R,VLBI}$	0.74	0.07

Note. Column (1)-(3): Variable X , Y and Z , respectively. Correlation between variables X and Y is studied, taking into account the mutual correlation of X and Y with the third variable Z . Column (4)-(5): the partial Kendall's correlation coefficient τ , and the probability for accepting the null hypothesis that there is no correlation between X and Y .

the nuclear monochromatic fluxes at 5100 Å after subtracting the starlight of the host galaxy (see references in Column 14 of Table 1). When the starlight-subtracted flux at 5100 Å is unavailable, we calculate L_{5100} using the measured $L_{H\beta}$ and the $L_{H\beta} - L_{5100}$ relation in Greene & Ho (2005). We note that the bolometric correction factor of 9.8 adopted here was measured based on a large sample of SDSS quasars (McLure & Dunlop 2004).

3 CORRELATION ANALYSIS

We plot X-ray luminosity versus radio luminosity in Figure 1. We calculate the Spearman's rank correlation coefficient ρ and the probability of null hypothesis (i.e., no correlations), P_{null} , to test whether there is significant correlations between the two variables, using the X-ray luminosities either in 2–10 keV or in 14–195 keV, and the radio luminosities calculated from either VLA or VLBI observations. However, all the tests give $P_{\text{null}} > 5\%$, which means that there is no significant correlation between the radio luminosity and X-ray luminosity.

By analyzing a large sample of AGNs, it was found that the radio luminosity depends on both the X-ray luminosity and black hole mass (e.g., Merloni et al. 2003). In the current paper, more generally, we explore the mutual relation between L_R , L_X , M_{BH} and nuclear monochromatic luminosity L_{5100} by using the partial

² Giacchè et al. (2014) have analyzed *XMM-Newton* observations on Mrk 766 between 2000 and 2005, and find the flux $F_{2-10\text{keV}}$ varied by a factor of ~ 5 with photon index between 0.95 and 2.1. But they suggest the X-ray emission is probably affected by occultations during $\Gamma < 1.6$. So we do not adopt the fluxes with $\Gamma < 1.6$.

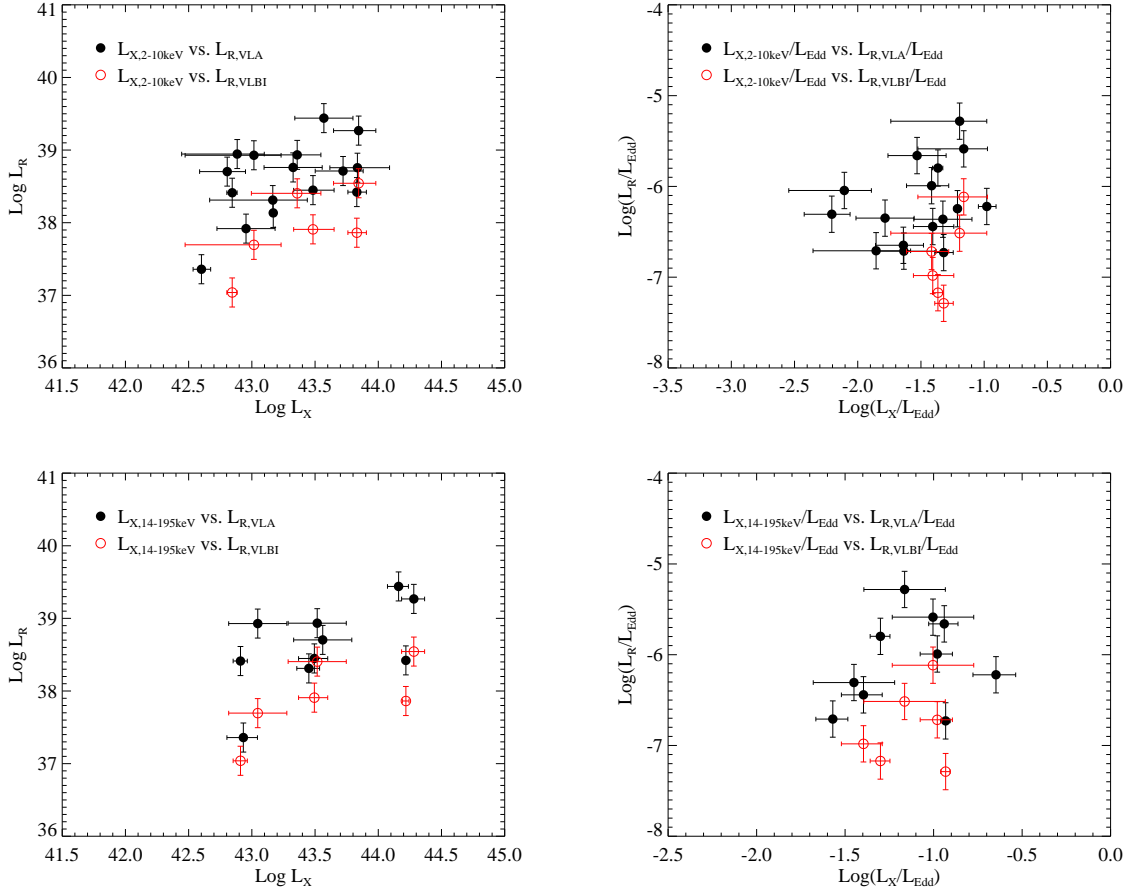


Figure 1. The $L_{X,2-10\text{keV}}$ versus L_R (upper left), $L_{X,2-10\text{keV}}/L_{\text{Edd}}$ versus L_R/L_{Edd} (upper right), $L_{X,14-195\text{keV}}$ versus L_R (lower left) and $L_{X,14-195\text{keV}}/L_{\text{Edd}}$ versus L_R/L_{Edd} (lower right). The VLA and VLBI data are represented by black filled circles and red open circles respectively.

Kendall's τ correlation test, which can be used to eliminate the effect of a third variable when assessing the correlation between two variables (Akritas & Siebert 1996).

Firstly, we calculate the partial correlation coefficients τ and the probabilities for null hypothesis P_{null} between either two of the radio luminosity L_R , X-ray luminosity L_X and optical luminosity L_{5100} , given that the black hole mass M_{BH} is the third variable. Only a weak correlation is revealed by the test between $L_{R,\text{VLA}}$ and L_{5100} with probability of $P_{\text{null}} = 4\%$. Then we test the correlations between L_X and L_R given that L_{5100} is the third variable. We don't find significant correlations between L_R and L_X in any cases so far. Finally, we test if there is correlation between L_R (or L_X) and M_{BH} , given that L_{5100} or L_X (or L_R) is the third variable. No significant correlation has been found between L_R and M_{BH} . However, both 2–10 keV and 14–195 keV luminosity significantly correlate with M_{BH} with $P_{\text{null}} < 1\%$.

In the left panel of Figure 2, we plot L_R versus L_{5100} using VLA and VLBI data respectively. It is clear that L_R increases with increasing L_{5100} . Then, as suggested by the partial correlation test (the fifth row of table 2), we plot the Eddington-scaled radio luminosity L_R/L_{Edd} versus the Eddington-scaled optical luminosity L_{5100}/L_{Edd} in the right panel of Figure 2. By adopting a typical uncertainty $\sigma_R = 0.2$ dex for the radio luminosity (Ho & Peng 2001),

the best-fitted linear relation using VLA data gives

$$\log\left(\frac{L_{R,\text{VLA}}}{L_{\text{Edd}}}\right) = (0.31 \pm 0.33) \log\left(\frac{L_{5100}}{L_{\text{Edd}}}\right) - (5.82 \pm 0.41). \quad (1)$$

In the left panel of Figure 3, we plot M_{BH} versus L_X using 2–10 keV luminosities and 14–195 keV luminosities respectively. The best-fitted linear relations of $M_{\text{BH}}-L_X$ are

$$\log L_{X,2-10\text{keV}} = (0.73 \pm 0.10) \log M_{\text{BH}} + (38.55 \pm 0.60) \quad (2)$$

and

$$\log L_{X,14-195\text{keV}} = (1.15 \pm 0.13) \log M_{\text{BH}} + (36.06 \pm 0.91). \quad (3)$$

In the right panel of Figure 3, as suggested by the partial correlation test (the seventh and eighth row of table 2), we plot the Eddington-scaled X-ray luminosity L_X/L_{Edd} versus the Eddington-scaled optical luminosity L_{5100}/L_{Edd} . No significant correlation between L_X/L_{Edd} and L_{5100}/L_{Edd} is found.

4 DISCUSSION

We collect the core radio luminosities calculated from high-resolution radio observations, as well as the X-ray luminosities for 16 nearby NLS1s with Eddington ratios $\gtrsim 0.1$. The high-resolution radio images avoid the host galaxy contamination as much as possible. Partial Kendall's τ correlation test is used to explore the mutual

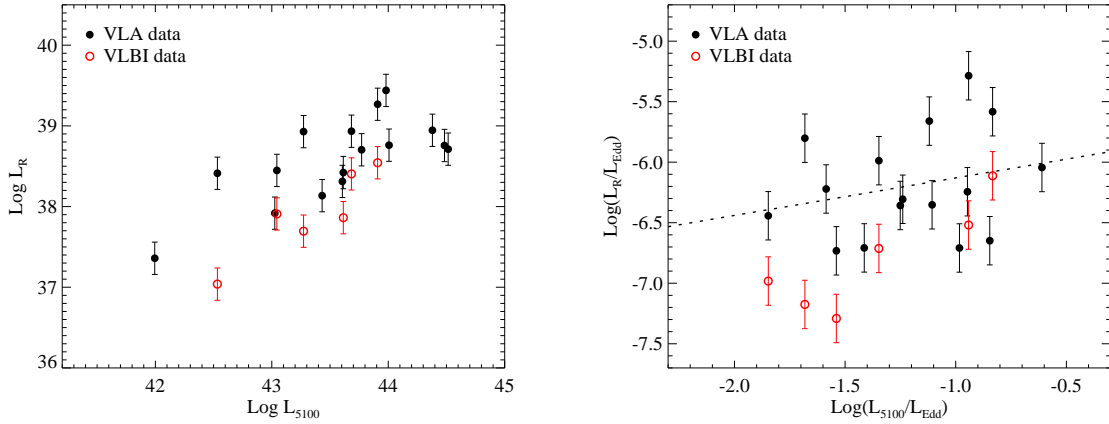


Figure 2. *Left panel:* The radio luminosity L_R versus the monochromatic nuclear optical luminosity L_{5100} . *Right panel:* L_R/L_{Edd} versus L_{5100}/L_{Edd} . The error bars represent typical uncertainties $\sigma_R = 0.2$ of the radio luminosities. The black dotted line in the right panel is the best linear fit to the relation of L_R/L_{Edd} and L_{5100}/L_{Edd} using VLA data.

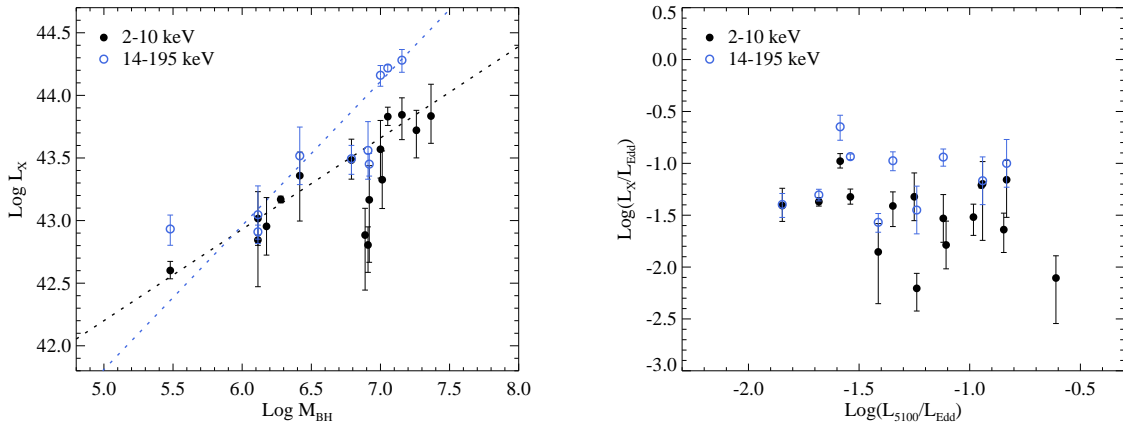


Figure 3. *Left panel:* The black filled circles and black dotted line represent respectively the $\log M_{\text{BH}}$ versus $\log L_X$ relation using 2 – 10 keV luminosity and the best linear fit, while the blue open circles and blue dotted line represent respectively the same relation using 14 – 195 keV luminosity and the best linear fit. *Right panel:* The Eddington-scaled optical luminosity L_{5100}/L_{Edd} versus the Eddington-scaled X-ray luminosity L_X/L_{Edd} in 2 – 10 keV and 14 – 195 keV, respectively.

relations between the radio luminosity, X-ray luminosity, nuclear optical luminosity and the black hole mass. As shown in Section 3, we don't find any significant correlations between the X-ray luminosity L_X , either in 2 – 10 keV or 14 – 195 keV, and the radio luminosity L_R , either using VLA data measured on scales of $\lesssim 1$ kpc or VLBI data measured on scales of a few pc. However, we find that there is a positive correlation between L_X and M_{BH} . Meanwhile, we find that there is no correlation between L_X/L_{Edd} and L_{5100}/L_{Edd} (right panel of Figure 3), which are suggested to be understood in the framework of slim disc scenario as follows.

The slim disc model has been proposed to explain the observational features of NLS1s in the past few decades (e.g., Abramowicz et al. 1988; Wang & Zhou 1999; Mineshige et al. 2000; Wang & Netzer 2003; Wang et al. 2013). In this model, when the accretion rate approaches or exceeds the Eddington limit, the disc within a certain radius R_{trap} becomes optically too thick that the time scale of the photon diffusion to the disc surface is longer than that of the viscous time scale of the accretion disc. In this case, most of the photons within this radius will be trapped in the disc un-

til advected into the black hole rather than being radiated out. The radius of the photon trapping region is dependent on the accretion rate as $R_{\text{trap}} \propto \dot{M}_{\text{disc}}$ (Wang & Zhou 1999; Wang et al. 2013). As \dot{M}_{disc} increases, the photon trapping region gets larger. The total luminosity of the slim disc is proportional logarithmically to \dot{M}_{disc} and eventually get saturated with increasing \dot{M}_{disc} . Then the total luminosity is independent on \dot{M}_{disc} and only depends on the black hole mass M_{BH} (Wang et al. 2013).

The hard X-ray emission above 2 keV in bright Seyfert galaxies and radio quiet quasars is believed to be from a so-called disc-corona system, which should be very similar in the case of NLS1s with a form of slim disc-corona system (e.g., Chen & Wang 2004; Jin et al. 2017). The emission from the disc mainly contributes to the optical/UV band, part of which will be Compton up-scattered in the hot corona, producing the hard X-ray emissions (e.g., Haardt & Maraschi 1991, 1993; Stern et al. 1995). Simply, the Compton cooling rate is determined by the following expres-

sions (Rybicki & Lightman 1986),

$$q_{\text{cooling}} = \frac{4kT_e}{m_e c^2} n_e \sigma_T c u, \quad (4)$$

where u is the seed photon energy density, T_e is the electron temperature, σ_T is the Thomson scattering cross section, n_e is the electron density and m_e is the electron mass. If the NLS1s in our sample are indeed powered by the slim disc-corona accretion, we will have a general consequence as follows. When the accretion rate gets near and above the Eddington limit as in the NLS1s studied here (Column 15 of Table 1), the emission from the accretion disc will be saturated and independent on the accretion rate within the photon trapping radius R_{trap} . Observationally, since the corona is very compact, located within less than ~ 20 gravitational radii of the black hole (e.g., Reis & Miller 2013), the covering factor of the accretion disc at the region beyond a few tens of gravitational radii as seen from the corona is very small. In this case, the seed photons to be intercepted and scattered in the corona will be mainly from the very innermost region of the accretion disc. So, in the slim disc scenario, although the luminosity of the accretion disc beyond R_{trap} do not get saturated, however, due to the relatively small contribution of the seed photon from this region, the seed photon energy density u for the inverse Compton scattering in the corona will not change much with increasing \dot{M}_{disc} . Meanwhile, if the property of the corona, such as the electron temperature and the optical depth also don't change, theoretically, the produced hard X-ray emission from the corona will not change much. Then the overall hard X-ray emission will be only dependent on the black hole mass, which is just the correlation we found between L_X and M_{BH} (left panel of Figure 3).

Physically, in the standard disc-corona case, the relative strength between the disc and the corona is determined by the relative mass accretion rate in the disc and corona. Generally, the radiation from the disc, L_{disc} , increases with an increase of the mass accretion rate in the disc, \dot{M}_{disc} , which will make the matter in the corona collapse due to the strong Compton cooling processes, decreasing the relative strength of the emission from the corona. In the slim disc-corona case, however, an increase of \dot{M}_{disc} does not increase the seed photon luminosity, which will not change the coronal luminosity, then consequently lead to the independence of the coronal luminosity on the accretion rate.

In summary, in the slim disc-corona scenario, with an increase of \dot{M}_{disc} , the disc luminosity increases, leading to an increase of L_{5100} . However, the X-ray luminosity nearly does not change. This is strongly supported by our finding in the current paper, i.e., there is no observed correlation between L_X/L_{Edd} and L_{5100}/L_{Edd} (right panel of Figure 3), meanwhile, there is a positive correlation between L_X and M_{BH} (left panel of Figure 3). We note that, in some numerical simulations of supercritical accretion flows, the fully saturated luminosity of the accretion disc occurs at Eddington ratio ~ 3 (e.g., Ohsuga et al. 2005), which is a little higher than that of the sources in our sample, i.e., 0.14–2.4 (Table 1). Obviously, when the Eddington ratio is in the range of 0.14 – 2.4, the disc is partly saturated, which can intrinsically predict our findings in Figure 3.

The relativistic jet has been widely observed in both AGNs and BHBs. So far, several models have been proposed for the jet formation, such as the Blandford-Znajek (BZ) process and Blandford-Payne (BP) process. In the BZ process, the jet is driven by extracting the rotational energy of the black hole via a large-scale magnetic field (Blandford & Znajek 1977). In the BP process, the magnetic fields thread the accretion disc, extracting the rotational energy of the accretion disc to drive the jet

(Blandford & Payne 1982). Some state-of-the-art numerical simulations of super-Eddington accretion around a supermassive black hole have been done for the formation of jet, in which the jet is driven by radiation pressure (e.g., Tchekhovskoy et al. 2014; Sądowski & Narayan 2015). We should note that, although a lot of important progresses have been made for the formation of the jet, we don't fully understand the physical mechanism for launching the jet yet (e.g., Romero et al. 2017).

As we know, a strong correlation between the radio luminosity and X-ray luminosity has been found both in AGNs and BHBs (e.g., Merloni et al. 2003). The advection dominated accretion flow (ADAF) plus jet model was proposed to explain the correlation, i.e., $L_R \propto L_X^{0.5-0.7}$ in LLAGNs and in the low/hard spectral state of BHBs for $L_X/L_{\text{Edd}} \lesssim 10^{-3}$ (e.g., Yuan & Cui 2005; Xie & Yuan 2016). The disc-corona plus jet was proposed to explain the correlation, i.e., $L_R \propto L_X^{1.4}$ for $L_X/L_{\text{Edd}} \gtrsim 10^{-3}$ in luminous AGNs and the luminous low/hard spectral state of BHBs (e.g., Dong et al. 2014; Qiao & Liu 2015). However, for the NLS1s in current paper, we don't find a significant correlation between the radio luminosity and X-ray luminosity, which may imply that the physics for the coupling between the accretion (especially the corona) and jet in NLS1s is completely different from other types of AGNs and the low/hard spectral state of BHBs. Due to the high Eddington ratios, NLS1s are argued to be the scale-up version of BHBs in their high/soft state or very high state (e.g., Arévalo et al. 2006). However, the relation between the radio and X-ray luminosities in the high/soft state or very high state of BHBs is not clear now (e.g., Rushton et al. 2016). Thus, we do not compare their radio-X-ray relations here.

In Merloni et al. (2003), different kinds of black hole sources were included to study the mutual dependencies of L_R , L_X and M_{BH} , including the BHBs in the low/hard spectral state, and different types of AGNs (LLAGNs, Seyfert galaxies and quasars). They have looked for the partial correlations between L_R and L_X by taking M_{BH} as the third variable. Then they have also looked for partial correlations between L_R (L_X) and M_{BH} by taking L_X (L_R) as the third variable. In their work, L_R is strongly correlated with both M_{BH} and L_X , and, in turn, L_X is correlated with both M_{BH} and L_R when both AGNs and BHBs are considered, which then leads to the discovery of the so-called ‘fundamental plane’. In our work, we only focus on a special subclass of AGNs, i.e., NLS1s, with relatively higher Eddington ratios. We don't find partial correlations between the radio luminosity and X-ray luminosity, and between the radio luminosity and black hole mass (Table 2). So the determination of a plane is impossible here. However, we find a significant partial correlation between the L_X and M_{BH} for NLS1s by taking L_R or L_{5100} as the third variable. This is in contrast with Merloni et al. (2003), in which L_X is found to be independent on M_{BH} when only AGNs are included (see their Table 2). This also implies that the coupling between the accretion and jet in the NLS1s is indeed different from other types of AGNs.

But we should note that, in the current paper, the number of the sources in the sample is small, which may make the statistical properties uncertain. A larger well-defined and uniformly selected sample with high resolution radio images and X-ray observations is needed to confirm our conclusions more robustly in the not far future.

ACKNOWLEDGEMENTS

We are grateful to anonymous referee for the helpful comments, which substantially improve the quality of this paper. We thank W. M. Yuan, B. F. Liu, Z. Liu, S. Komossa and H. Y. Zhou for helpful discussions. This work has made use of the NED which is operated by the Jet Propulsion Laboratory, California Institute of Technology, under contract with the National Aeronautics and Space Administration. S. Yao thanks the supported by KIAA-CAS fellowship. E. L. Qiao thanks the supports by the NSFC grant No. 11773037. X. B. Wu thanks the supports by the Ministry of Science and Technology of China under grant 2016YFA0400703, the NSFC grants No.11373008 and 11533001, and the National Key Basic Research Program of China 2014CB845700.

REFERENCES

- Abdo A. A., et al., 2009a, *ApJ*, **699**, 976
 Abdo A. A., et al., 2009b, *ApJ*, **707**, L142
 Abramowicz M. A., Czerny B., Lasota J. P., Szuszkiewicz E., 1988, *ApJ*, **332**, 646
 Akritas M. G., Siebert J., 1996, *MNRAS*, **278**, 919
 Arévalo P., Papadakis I. E., Uttley P., McHardy I. M., Brinkmann W., 2006, *MNRAS*, **372**, 401
 Baumgartner W. H., Tueller J., Markwardt C. B., Skinner G. K., Barthelmy S., Mushotzky R. F., Evans P. A., Gehrels N., 2013, *ApJS*, **207**, 19
 Berton M., et al., 2015, *A&A*, **578**, A28
 Bianchi S., Guainazzi M., Matt G., Fonseca Bonilla N., Ponti G., 2009, *A&A*, **495**, 421
 Blandford R. D., Payne D. G., 1982, *MNRAS*, **199**, 883
 Blandford R. D., Znajek R. L., 1977, *MNRAS*, **179**, 433
 Boissay R., Ricci C., Paltani S., 2016, *A&A*, **588**, A70
 Boller T., Brandt W. N., Fink H., 1996, *A&A*, **305**, 53
 Boroson T. A., 2002, *ApJ*, **565**, 78
 Boroson T. A., Green R. F., 1992, *ApJS*, **80**, 109
 Botte V., Ciroi S., Rafanelli P., Di Mille F., 2004, *AJ*, **127**, 3168
 Brightman M., Nandra K., 2011, *MNRAS*, **413**, 1206
 Caccianiga A., et al., 2015, *MNRAS*, **451**, 1795
 Chen L.-H., Wang J.-M., 2004, *ApJ*, **614**, 101
 Corbel S., Fender R. P., Tomsick J. A., Tzioumis A. K., Tingay S., 2004, *ApJ*, **617**, 1272
 Costantini E., Gallo L. C., Brandt W. N., Fabian A. C., Boller T., 2007, *MNRAS*, **378**, 873
 Czerny B., You B., 2016, *Astronomische Nachrichten*, **337**, 73
 D’Ammando F., et al., 2012, *MNRAS*, **426**, 317
 Denney K. D., et al., 2009, *ApJ*, **702**, 1353
 Deo R. P., Crenshaw D. M., Kraemer S. B., 2006, *AJ*, **132**, 321
 Doi A., Asada K., Nagai H., 2011, *ApJ*, **738**, 126
 Doi A., Nagai H., Kawakatu N., Kino M., Nagai H., Asada K., 2012, *ApJ*, **760**, 41
 Doi A., Asada K., Fujisawa K., Nagai H., Hagiwara Y., Wajima K., Inoue M., 2013, *ApJ*, **765**, 69
 Doi A., Wajima K., Hagiwara Y., Inoue M., 2015, *ApJ*, **798**, L30
 Dong A.-J., Wu Q., Cao X.-F., 2014, *ApJ*, **787**, L20
 Fabbiano G., 1989, *ARA&A*, **27**, 87
 Falcke H., Sherwood W., Patnaik A. R., 1996, *ApJ*, **471**, 106
 Foschini L., et al., 2015, *A&A*, **575**, A13
 Fukazawa Y., et al., 2011, *ApJ*, **727**, 19
 Gallo L. C., Balestra I., Costantini E., Boller T., Burwitz V., Ferrero E., Mathur S., 2005, *A&A*, **442**, 909
 George I. M., Turner T. J., Yaqoob T., Netzer H., Laor A., Mushotzky R. F., Nandra K., Takahashi T., 2000, *ApJ*, **531**, 52
 Giacchè S., Gilli R., Titarchuk L., 2014, *A&A*, **562**, A44
 Giroletti M., Panessa F., 2009, *ApJ*, **706**, L260
 Goodrich R. W., 1989, *ApJ*, **342**, 224
 Greene J. E., Ho L. C., 2005, *ApJ*, **630**, 122
 Grier C. J., et al., 2013, *ApJ*, **773**, 90
 Grupe D., Mathur S., Komossa S., 2004, *AJ*, **127**, 3161
 Grupe D., Komossa S., Gallo L. C., 2007, *ApJ*, **668**, L111
 Grupe D., Komossa S., Leighly K. M., Page K. L., 2010, *ApJS*, **187**, 64
 Gu M., Chen Y., Komossa S., Yuan W., Shen Z., Wajima K., Zhou H., Zensus J. A., 2015, *ApJS*, **221**, 3
 Haardt F., Maraschi L., 1991, *ApJ*, **380**, L51
 Haardt F., Maraschi L., 1993, *ApJ*, **413**, 507
 Ho L. C., Peng C. Y., 2001, *ApJ*, **555**, 650
 Ho L. C., Ulvestad J. S., 2001, *ApJS*, **133**, 77
 Ho L. C., Darling J., Greene J. E., 2008, *ApJS*, **177**, 103
 Inoue H., Terashima Y., Ho L. C., 2007, *ApJ*, **662**, 860
 Ivezić Ž., et al., 2002, *AJ*, **124**, 2364
 Iwasawa K., Brandt W. N., Fabian A. C., 1998, *MNRAS*, **293**, 251
 Jin C., Done C., Middleton M., Ward M., 2013, *MNRAS*, **436**, 3173
 Jin C., Done C., Ward M., 2017, *MNRAS*, **468**, 3663
 Keek L., Ballantyne D. R., 2016, *MNRAS*, **456**, 2722
 Kellermann K. I., Sramek R., Schmidt M., Shaffer D. B., Green R., 1989, *AJ*, **98**, 1195
 Kellermann K. I., Sramek R. A., Schmidt M., Green R. F., Shaffer D. B., 1994, *AJ*, **108**, 1163
 Kinney A. L., Schmitt H. R., Clarke C. J., Pringle J. E., Ulvestad J. S., Antonucci R. R. J., 2000, *ApJ*, **537**, 152
 Komossa S., Voges W., Xu D., Mathur S., Adorf H.-M., Lemson G., Duschl W. J., Grupe D., 2006, *AJ*, **132**, 531
 Körding E., Falcke H., Corbel S., 2006, *A&A*, **456**, 439
 Kukula M. J., Pedlar A., Baum S. A., O’Dea C. P., 1995, *MNRAS*, **276**, 1262
 Kukula M. J., Dunlop J. S., Hughes D. H., Rawlings S., 1998, *MNRAS*, **297**, 366
 Lal D. V., Shastri P., Gabuzda D. C., 2004, *A&A*, **425**, 99
 Landi R., Malizia A., Bassani L., 2005, *A&A*, **441**, 69
 Leighly K. M., Moore J. R., 2004, *ApJ*, **611**, 107
 Li Z.-Y., Wu X.-B., Wang R., 2008, *ApJ*, **688**, 826
 Liu B. F., Mineshige S., Meyer F., Meyer-Hofmeister E., Kawaguchi T., 2002, *ApJ*, **575**, 117
 Liu T., Wang J.-X., Yang H., Zhu F.-F., Zhou Y.-Y., 2014, *ApJ*, **783**, 106
 Liu Z., Yuan W., Lu Y., Zhou X., 2015, *MNRAS*, **447**, 517
 Lutz D., Maiolino R., Spoon H. W. W., Moorwood A. F. M., 2004, *A&A*, **418**, 465
 Marziani P., Sulentic J. W., Zamanov R., Calvani M., Dultzin-Hacyan D., Bachev R., Zwitter T., 2003, *ApJS*, **145**, 199
 Matsumoto C., Leighly K. M., Marshall H. L., 2004, *ApJ*, **603**, 456
 Matt G., Perola G. C., Fiore F., Guainazzi M., Nicastro F., Piro L., 2000, *A&A*, **363**, 863
 McLure R. J., Dunlop J. S., 2004, *MNRAS*, **352**, 1390
 Merloni A., Heinz S., di Matteo T., 2003, *MNRAS*, **345**, 1057
 Miller P., Rawlings S., Saunders R., 1993, *MNRAS*, **263**, 425
 Mineshige S., Kawaguchi T., Takeuchi M., Hayashida K., 2000, *PASJ*, **52**, 499
 Mushotzky R. F., Done C., Pounds K. A., 1993, *ARA&A*, **31**, 717
 Nandra K., O’Neill P. M., George I. M., Reeves J. N., 2007, *MNRAS*, **382**, 194
 Ohsuga K., Mori M., Nakamoto T., Mineshige S., 2005, *ApJ*, **628**, 368
 Ohta K., Aoki K., Kawaguchi T., Kiuchi G., 2007, *ApJS*, **169**, 1
 Orienti M., Prieto M. A., 2010, *MNRAS*, **401**, 2599
 Osterbrock D. E., Pogge R. W., 1985, *ApJ*, **297**, 166
 Panessa F., et al., 2011, *MNRAS*, **417**, 2426
 Panessa F., et al., 2015, *MNRAS*, **447**, 1289
 Papadakis I. E., Brinkmann W., Page M. J., McHardy I., Uttley P., 2007, *A&A*, **461**, 931
 Parra R., Conway J. E., Aalto S., Appleton P. N., Norris R. P., Pihlström Y. M., Kewley L. J., 2010, *ApJ*, **720**, 555
 Piconcelli E., Jimenez-Bailón E., Guainazzi M., Schartel N., Rodríguez-Pascual P. M., Santos-Lleó M., 2005, *A&A*, **432**, 15
 Qiao E., Liu B. F., 2015, *MNRAS*, **448**, 1099
 Ramírez J. M., 2013, *A&A*, **551**, A95
 Reeves J. N., Turner M. J. L., 2000, *MNRAS*, **316**, 234

- Reis R. C., Miller J. M., 2013, *ApJ*, **769**, L7
- Romero G. E., Boettcher M., Markoff S., Tavecchio F., 2017, *Space Sci. Rev.*, **207**, 5
- Rushton A., Spencer R., Fender R., Pooley G., 2010, *A&A*, **524**, A29
- Rushton A. P., et al., 2016, *MNRAS*, **463**, 628
- Ryan C. J., De Robertis M. M., Virani S., Laor A., Dawson P. C., 2007, *ApJ*, **654**, 799
- Rybicki G. B., Lightman A. P., 1986, *Radiative Processes in Astrophysics*
- Sani E., Lutz D., Risaliti G., Netzer H., Gallo L. C., Trakhtenbrot B., Sturm E., Boller T., 2010, *MNRAS*, **403**, 1246
- Sądowski A., Narayan R., 2015, *MNRAS*, **453**, 3213
- Schmitt H. R., Ulvestad J. S., Antonucci R. R. J., Kinney A. L., 2001, *ApJS*, **132**, 199
- Shinozaki K., Miyaji T., Ishisaki Y., Ueda Y., Ogasaka Y., 2006, *AJ*, **131**, 2843
- Shu X. W., Yaqoob T., Wang J. X., 2010, *ApJS*, **187**, 581
- Stepanian J. A., et al., 2003, *ApJ*, **588**, 746
- Stern B. E., Poutanen J., Svensson R., Sikora M., Begelman M. C., 1995, *ApJ*, **449**, L13
- Strateva I. V., Brandt W. N., Schneider D. P., Vanden Berk D. G., Vignali C., 2005, *AJ*, **130**, 387
- Sulentic J. W., Zwitter T., Marziani P., Dultzin-Hacyan D., 2000, *ApJ*, **536**, L5
- Sulentic J. W., Bachev R., Marziani P., Negrete C. A., Dultzin D., 2007, *ApJ*, **666**, 757
- Tchekhovskoy A., Metzger B. D., Giannios D., Kelley L. Z., 2014, *MNRAS*, **437**, 2744
- Thean A., Pedlar A., Kukula M. J., Baum S. A., O’Dea C. P., 2001, *MNRAS*, **325**, 737
- Turner T. J., Romano P., George I. M., Edelson R., Collier S. J., Mathur S., Peterson B. M., 2001, *ApJ*, **561**, 131
- Ueda Y., Ishisaki Y., Takahashi T., Makishima K., Ohashi T., 2001, *ApJS*, **133**, 1
- Ulvestad J. S., Wilson A. S., 1984a, *ApJ*, **278**, 544
- Ulvestad J. S., Wilson A. S., 1984b, *ApJ*, **285**, 439
- Ulvestad J. S., Antonucci R. R. J., Goodrich R. W., 1995, *AJ*, **109**, 81
- Véron-Cetty M.-P., Véron P., 2010, *A&A*, **518**, A10
- Véron-Cetty M.-P., Véron P., Gonçalves A. C., 2001, *A&A*, **372**, 730
- Vestergaard M., Peterson B. M., 2006, *ApJ*, **641**, 689
- Vignali C., Brandt W. N., Boller T., Fabian A. C., Vaughan S., 2004, *MNRAS*, **347**, 854
- Wang T., Lu Y., 2001, *A&A*, **377**, 52
- Wang J.-M., Netzer H., 2003, *A&A*, **398**, 927
- Wang J.-M., Zhou Y.-Y., 1999, *ApJ*, **516**, 420
- Wang T., Brinkmann W., Bergeron J., 1996, *A&A*, **309**, 81
- Wang R., Wu X.-B., Kong M.-Z., 2006, *ApJ*, **645**, 890
- Wang J.-M., Du P., Valls-Gabaud D., Hu C., Netzer H., 2013, *Physical Review Letters*, **110**, 081301
- Wang J.-M., et al., 2014, *ApJ*, **793**, 108
- Whalen D. J., Laurent-Muehleisen S. A., Moran E. C., Becker R. H., 2006, *AJ*, **131**, 1948
- Winter L. M., Veilleux S., McKernan B., Kallman T. R., 2012, *ApJ*, **745**, 107
- Xie F.-G., Yuan F., 2016, *MNRAS*, **456**, 4377
- Yao S., Yuan W., Zhou H., Komossa S., Zhang J., Qiao E., Liu B., 2015, *MNRAS*, **454**, L16
- Yuan F., Cui W., 2005, *ApJ*, **629**, 408
- Yuan W., Zhou H. Y., Komossa S., Dong X. B., Wang T. G., Lu H. L., Bai J. M., 2008, *ApJ*, **685**, 801
- Zhou H., Wang T., Yuan W., Lu H., Dong X., Wang J., Lu Y., 2006, *ApJS*, **166**, 128
- de Gasperin F., Merloni A., Sell P., Best P., Heinz S., Kauffmann G., 2011, *MNRAS*, **415**, 2910
- de La Calle Pérez I., et al., 2010, *A&A*, **524**, A50

This paper has been typeset from a \LaTeX file prepared by the author.